THE JOURNAL OF PHYSICAL CHEMISTRY C

Article

Cite This: J. Phys. Chem. C 2019, 123, 13304−13317

pubs.acs.org/JPCC

Modeling Electron Transfer in Diffusive Multidimensional Electrochemical Systems

Alec J. Coffman,*[,†] Aparna Karippara Harshan,[‡] Sharon Hammes-Schiffer,[§] and Joseph E. Subotnik[†]

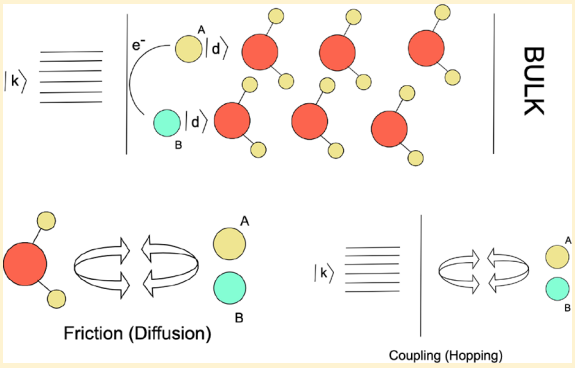
[†]Department of Chemistry, University of Pennsylvania, Philadelphia, Pennsylvania 19104, United States

[‡]Department of Chemistry, University of Illinois at Urbana-Champaign, Urbana, Illinois 61801, United States

[§]Department of Chemistry, Yale University, New Haven, Connecticut 06520, United States

Supporting Information

ABSTRACT: We analyze different stochastic approaches for simulating electron transfer and potential sweep experiments in diffusive multidimensional electrochemical systems. In particular, we focus on a simple two-dimensional system, where one dimension is a traditional mass diffusion coordinate moving reactants from bulk solution to an electrode, and a second dimension represents a reorganization coordinate capturing solvent motion. We find that this multidimensional system can indeed be reduced to a simpler one-dimensional model, provided certain circumstances pertaining to separability between the two coordinates are met. Our results should begin to bridge the gap between continuum models of electrochemical dynamics/transport and ab initio models of surface electronic structure.



1. INTRODUCTION

Within the field of electrochemistry, one of the open questions is: what is the simplest computational model for capturing the details of Tafel plots and cyclic voltammograms (CV) for realistic experiments? Historically, when modeling such electron transfer (ET) events at the electrode surface, the usual approach has been to enforce either static or local empirical boundary conditions, especially the Nernstian equilibrium or Butler−Volmer kinetics.[1] These boundary conditions are simple to implement and applicable in many common applications, even in the presence of diffuse charges on surfaces.[2] Nevertheless, the above approaches do not address the actual mechanism of a complicated ET event;[3] for instance, the Butler−Volmer approach hides a great deal of physics (all barrier heights and shapes, reorganization free energies, solvent recrossing probabilities) in one empirical parameter, namely, the transfer coefficient.

Many efforts to improve upon the canonical techniques of electrochemistry have been constructed, most commonly using the Marcus−Hush (MH) theory which usually assumes symmetric parabolas.[4,5] However, there have also been some developments for asymmetric parabolas[6] and nonparabolic surfaces (where local low-frequency vibrations can alter the effective force constant of the two oxidative states differently[7]). More generally, one can estimate rate constants for the electron transfer using Fermi's golden rule and evaluating a one-dimensional (1D) integral (sometimes called the Marcus−Hush−Chidsey integral[8,9]). And quite often, by fitting experimental $I-V$ curves to Fermi's golden rule (FGR) rates, one can extract reasonable thermodynamic parameters, e.g., reorganization energies.[10] However, even this approach is not without limitations,[11] and FGR integrals have been shown to be insufficient for replicating some voltammetry experiments quantitatively;[6] in fact, sometimes, more involved FGR treatments of $I-V$ curves perform worse than the simpler Butler−Volmer equations.[12] Current electrochemical research is exploring alternatives to Butler−Volmer, including phase-field models,[13] density functional theory (DFT)-aided molecular dynamics simulations,[14,15] and other approaches.

In the end, the potential energy surfaces as relevant to electrochemistry are large and quite complicated, and the statistical mechanics of sampling such configurations is daunting. As far as we are aware, there is still no complete and practical methodology for simulating electrochemical phenomena that (i) can describe complex chemical transformations (including multielectron transfer events) using (ii) only a few parameters (ideally extracted from electronic structure theory). We also note that modern simulations using the Nernstian and Butler−Volmer boundary conditions should be valid only when the electron transfer at the surface is relatively fast and largely decoupled from other surface processes. Unlike these approaches, the ideal electrochemical simulation (iii) should be applicable whether electron transfer, mass diffusion, or some other transformation is rate limiting. From our point of view, even though there is also a long history of studying ET coupled to diffusion in solution[16−19] as

Received: March 4, 2019
Revised: April 26, 2019
Published: May 1, 2019

Downloaded by UNIV OF PENNSYLVANIA at 13:52:41:742 on June 08, 2019
from https://pubs.acs.org/doi/10.1021/acs.jpcc.9b02068.

© 2019 American Chemical Society

DOI: 10.1021/acs.jpcc.9b02068
J. Phys. Chem. C 2019, 123, 13304−13317

well as photoinduced ET and ion recombination in different enviornments,[20−22] there has still been very little development of the theory of electrochemical dynamics compared to the vast theoretical developments in photochemistry and photodynamics. This gap between photochemistry and electrochemistry poses both challenges and opportunities for chemical theory. Recently, there has been recognition of the importance of modeling the electrochemical ET through a more complete Marcus picture,[23] but previous works in this vein have usually assumed restrictive conditions, for example, focusing primarily on equilibrium statistical fluctuations.[24] Thus far, little attention has been given to methods that explicitly model the dynamics of electrochemical ET with molecular motion in bulk and at the surface.

In this paper, we analyze the simplest such multidimensional approach for simulating electrochemical dynamics: we study electron transfer with molecular motion possible along two different nuclear coordinates, one a solvent reorganization coordinate and the other a diffusion coordinate, under an applied potential. By modeling ET with a stochastic, nonadiabatic surface hopping[25] (SH) ansatz, we will build new intuition for how to understand $I-V$ curves dynamically. An outline of this paper is as follows. In Section 2, we compare the standard approaches for electrochemical simulations, highlighting how these different approaches relate to one another. In Section 3, we present results for each approach, comparing and contrasting when a two-dimensional (2D) simulation can be reduced to a more simpler one-dimensional case. Finally, in Section 4, we discuss how to connect mass transport models with ab initio models of electrochemical dynamics and we point out the obvious improvements needed to make progress. We conclude in Section 5.

2. METHODS

2.1. Basic Electrochemical Methods in One Dimension. As is standard, we begin our discussion with an analysis of electrochemical dynamics in one dimension, where mass transport and diffusion are paramount.

2.1.1. Mass Transport with Butler−Volmer and Nernstian Boundary Conditions. Historically, the simulation of electrochemical systems has been carried out by modeling solute mass transport and incorporating electrode boundary conditions that obey either Nernstian or Butler−Volmer boundary conditions. For the most part, this approach requires only a simple grid in one dimension (to simulate the diffusive motion of the electroactive species in the solution) and the implementation of species exchange at the surface (to simulate charge transfer).

To illustrate this approach, consider the following equation

$$\mathrm{A} + \mathrm{e}^- \underset{k_\mathrm{b}}{\overset{k_\mathrm{f}}{\rightleftharpoons}} \mathrm{B}$$

Here, species A is reduced at the electrode to form B, and the reaction is reversible. The kinetics obeys

$$\vec{J}_\mathrm{A} = -D_\mathrm{A}^x \frac{\partial c_\mathrm{A}}{\partial x}\hat{x}$$
$$\vec{J}_\mathrm{B} = -D_\mathrm{B}^x \frac{\partial c_\mathrm{B}}{\partial x}\hat{x} \tag{1a}$$

$$\frac{\partial c_\mathrm{A}}{\partial t} = -\vec{\nabla}\cdot\vec{J}_\mathrm{A} = D_\mathrm{A}^x \frac{\partial^2 c_\mathrm{A}}{\partial x^2}$$
$$\frac{\partial c_\mathrm{B}}{\partial t} = -\vec{\nabla}\cdot\vec{J}_\mathrm{B} = D_\mathrm{B}^x \frac{\partial^2 c_\mathrm{B}}{\partial x^2} \tag{1b}$$

where $\hat{x}$ is the unit vector for the diffusive coordinate, J_A (J_B) is the current of species A (B), and D_A^x (D_B^x) is the diffusion coefficient in the x-direction (which we take as equal for both species A and B). Equations 1a and 1b are an almost complete protocol for simulating electrochemical systems but does require boundary conditions. The system is governed by the following initial conditions

$$c_\mathrm{A}(t=0, x) = c_\mathrm{A}^\mathrm{bulk} = 1 \tag{2a}$$

$$c_\mathrm{B}(t=0, x) = c_\mathrm{B}^\mathrm{bulk} = 0 \tag{2b}$$

and bath boundary conditions

$$c_\mathrm{A}(t, x=\infty) = c_\mathrm{A}^\mathrm{bulk} = 1 \tag{3a}$$

$$c_\mathrm{B}(t, x=\infty) = c_\mathrm{B}^\mathrm{bulk} = 0 \tag{3b}$$

The initial conditions above state that only A is present at time zero and the boundary conditions are defined so that the concentrations of A and B are equal to their bulk concentrations infinitely far from the electrode. What remains to be determined, however, are the dynamical boundary conditions at the electrode surface, where two options are standard.

2.1.1.1. Nernstian. On the one hand, Nernstian boundary conditions enforce the proper equilibrium ratio for the surface concentration of the species A divided by the surface concentration of the species B at all times. We assume that the surface concentrations at the boundary are related to the ratio of the forward and backward rate constants, k_f and k_b[1,26]

$$\frac{c_\mathrm{B}}{c_\mathrm{A}}\Big|_{x=0} = \frac{k_\mathrm{f}}{k_\mathrm{b}} = \mathrm{e}^{-\beta(\Delta G(t)-\Delta G^\circ)} \tag{4}$$

2.1.1.2. Butler−Volmer. On the other hand, Butler−Volmer boundary conditions stipulate that the concentration gradient at the electrode surface must be equal to the net flux

$$D_\mathrm{A}^x \frac{\partial c_\mathrm{A}}{\partial x}\Big|_{x=0} = k_\mathrm{f} c_\mathrm{A}|_{x=0} - k_\mathrm{b} c_\mathrm{B}|_{x=0} \tag{5}$$

The forward and backward rates are given by

$$k_\mathrm{f} = k^\circ \mathrm{e}^{-\alpha\beta(\Delta G(t)-\Delta G^\circ)} \tag{6a}$$

$$k_\mathrm{b} = k^\circ \mathrm{e}^{(1-\alpha)\beta(\Delta G(t)-\Delta G^\circ)} \tag{6b}$$

where k° is the standard rate constant, α is the transfer coefficient, $\beta = (kT)^{-1}$, $\Delta G(t)$ is the external potential, and ΔG° is the redox potential of the A/B redox couple.[1,26] In the standard electrochemical literature, the value of the transfer coefficient is usually related to the symmetry of the energy barrier in going from A to B and is equal to 0.5 in the case where the barrier from A to B is completely symmetric. For both Nernstian and Butler−Volmer dynamics, we also assume that the flux of species A and B are equal and opposite at the electrode, $J_\mathrm{A} = -J_\mathrm{B}$. When supplemented with one more equation to ensure mass conservation, the above equations define either Nernstian (eq 4) or Butler−Volmer (eqs 5, 6a,

DOI: 10.1021/acs.jpcc.9b02068
J. Phys. Chem. C 2019, 123, 13304−13317

and 6b) electrochemical dynamics. For more details about the implementation of these conditions, see Appendix C.

Solving the above boundary value problem has a long history, attempted first by Randles[27] and Ševčík.[28] In the case of Nernstian dynamics for a linear sweep voltammetry experiment, there exist analytical values for the peak current and peak potential, I_p and ΔG_p, found by Laplace transforming the diffusion equations in eq 1b and employing the boundary conditions in eqs 2a, 2b, 3a, 3b, and 4.[29] Assuming units of current in amperes, electrode area A in cm^2, diffusion constant D in cm^2/s, the scan rate ν in V/s, and concentration c_A in mol/cm^3, one arrives at

$$I_p = (2.69 \times 10^5) n^{3/2} A D_A^{1/2} \nu^{1/2} c_A(t = 0) \tag{7}$$

for the peak current and

$$\Delta G_p = \Delta G_{p/2} - 2.20 \frac{RT}{n\mathcal{F}} \tag{8}$$

for the peak potential (in V). Here, n is the number of electrons transferred in the ET event, $\mathcal{F}$ is the Faraday constant, and $\Delta G_{p/2}$ is the half-peak potential,[1] i.e., the driving force for which the current is half of the maximum current in eq 7. Equation 7 shows that for Nernstian systems where ET kinetics is reversible, I_p is proportional to $\nu^{1/2}$ and does not depend on k°. For systems that exhibit more complicated dynamics than those of the reversible case, the values of I_p and ΔG_p become more complicated functions of a unitless parameter,[30] which can be seen as a measure of the relative rates of ET kinetics (k°) and mass transfer kinetics $\left(\sqrt{\frac{D\nu\mathcal{F}}{RT}}\right)$. The statements above can be extended beyond linear sweeps to the case of cyclic voltammetry, although again, exact analytical expressions exist only for the Nernstian case.[31,32]

2.1.2. Generalized SH Approach with Flexible Boundary Conditions. The Butler–Volmer dynamics described above shows similarities to a stochastic master equation approach. In fact, with a little work, it can be easily shown that eqs 1a, 1b, and 5 are identical to classical surface hopping solving for the dynamics of coupled nuclear and electronic motion near a metal surface. To be precise, consider the following generalized Anderson–Holstein (AH) Hamiltonian, where an electronic impurity (i.e., a redox-active molecule) is coupled to a collection of nuclei (with position $\hat{q}_\alpha$ and momentum $\hat{\Pi}_\alpha$ and $[\hat{q}_\alpha, \hat{\Pi}_\alpha] = i\hbar$) and a bath of metallic fermions (indexed by k)

$$H = H_s + H_b + H_c \tag{9a}$$

$$H_s = E(\vec{r}) d^\dagger d + U_A(\vec{r}) + \frac{\vec{p}\cdot\vec{p}}{2m} + H_p \tag{9b}$$

$$H_p = \sum_\alpha \left[\frac{1}{2}\left(\frac{\Pi_\alpha^2}{m_\alpha} + m_\alpha \omega_\alpha^2 q_\alpha^2 \right) + \left(g_\alpha q_\alpha \vec{r} + \frac{(g_\alpha \vec{r})^2}{2 m_\alpha \omega_\alpha^2} \right) \right] \tag{9c}$$

$$H_b = \sum_k (\epsilon_k - \mu) c_k^\dagger c_k \tag{9d}$$

$$H_c = \sum_k W_k(\vec{r})(c_k^\dagger d + d^\dagger c_k) \tag{9e}$$

Here, H_s represents a Hamiltonian for a molecule with molecular orbital d near a metal surface; H_p represents a collection of nuclear coordinates that lead to a friction for the molecule; H_b represents a metal surface with multiple electronic states, indexed by k; and H_c represents the coupling between electrons in the metal and the molecule. $\vec{r}$ is the position operator for the electronic impurity; in principle, $\vec{r}$ in eqs 9b, 9c, and 9e represents a multidimensional nuclear coordinate, however, in one dimension, $\vec{r}$ becomes a scalar variable x. g_α is the coupling between the molecule and the collection of nuclei indexed by coordinate α, $d/d^\dagger$ represents creation and annihilation operators for a molecular orbital near a surface, μ is the chemical potential of the metal, $c_k/c_k^\dagger$ are the annihilation and creation operators for the metallic bath of electronic states, and W_k is the coupling between the electronic bath and the molecular orbital d. In practice, we will use the function Γ

$$\Gamma(\vec{r}, \epsilon) = 2\pi \sum_k |W_k(\vec{r})|^2 \delta(\epsilon_k - \epsilon) \tag{10}$$

to characterize the strength of the electron–metal coupling, where $\frac{\hbar}{\Gamma}$ is the lifetime of an electron placed on the molecule. In the wide band limit, one can assume that $\Gamma(\vec{r}, \epsilon)$ depends only on $\vec{r}$ (and not on ϵ).

The model in eqs 9a, 9b, 9c, 9d, and 9e incorporates two potential energy surfaces (PESs): we define U_A to be the diabatic PES for the case where the impurity is unoccupied and we define U_B to be the diabatic PES for the case where the impurity is occupied. Thus, the function E in eq 9b can be defined as the difference between the diabatic states, $E(\vec{r}) \equiv U_B(\vec{r}) - U_A(\vec{r})$. Furthermore, in one dimension, it is standard to choose flat potential energy surfaces with no x dependence[a], such that

$$U_B \equiv U_A + \Delta G \tag{11a}$$

$$E = \Delta G \tag{11b}$$

2.1.2.1. Classical Master Equation (CME) for Solving the AH Model. As shown in ref 34, if we consider the limit of weak coupling Γ and high temperature (where all nuclear motions are classical) and the limit of strong friction, so that all translational motions are diffusive and governed by the Smoluchowski equation, one can propagate dynamics for the Hamiltonian in eqs 9a, 9b, 9c, 9d, and 9e by solving the relevant master equation of the form

$$\frac{\partial c_A}{\partial t} = -\vec{\nabla}\cdot\overrightarrow{J_A} - (k_f c_A - k_b c_B)\delta(x) = D_A^x \frac{\partial^2 c_A}{\partial x^2} - (k_f c_A - k_b c_B)\delta(x) \tag{12a}$$

$$\frac{\partial c_B}{\partial t} = -\vec{\nabla}\cdot\overrightarrow{J_B} + (k_f c_A - k_b c_B)\delta(x) = D_B^x \frac{\partial^2 c_B}{\partial x^2} + (k_f c_A - k_b c_B)\delta(x) \tag{12b}$$

Here, we have assumed $\Gamma(x) = \Gamma_0\delta(x)$ so that all hoppings occur at only $x = 0$. The relevant electrode and bath boundary conditions are

$$c_A(t, x = -1) = c_A(t, x = 0) \tag{13a}$$

$$c_B(t, x = -1) = c_B(t, x = 0) \tag{13b}$$

DOI: 10.1021/acs.jpcc.9b02068
J. Phys. Chem. C 2019, 123, 13304–13317

$$c_A(t, x = \infty) = 1 \tag{13c}$$

$$c_B(t, x = \infty) = 0 \tag{13d}$$

Here, we have invoked a fictitious boundary point at $x = -1$[b]. In principle, eqs 12a and 12b can be solved by sampling over a swarm of trajectories hopping back and forth between surfaces and undergoing stochastic motion with Langvein forces. However, to save time, we will integrate eqs 12a and 12b directly, solving for the time dependence of the probability densities as they are propagated with the coupled Smoluchowski equations.

Now, to prove the equivalence between eqs 1a, 1b, 5, 12a, and 12b, we simply integrate both sides of eqs 12a and 12b over a small length ϵ, where $\epsilon \to 0$

$$\int_{-\epsilon}^{\epsilon} \frac{\partial c_A}{\partial t}\,dx = \int_{-\epsilon}^{\epsilon} (D_A^x \frac{\partial^2 c_A}{\partial x^2} - (k_f c_A + k_b c_B)\delta(x))\,dx$$

$$0 = D_A \frac{\partial c_A}{\partial x}|_{x=0} - k_f c_A|_{x=0} + k_b c_B|_{x=0} \tag{14a}$$

$$\int_{-\epsilon}^{\epsilon} \frac{\partial c_B}{\partial t}\,dx = \int_{-\epsilon}^{\epsilon} (D_B \frac{\partial^2 c_B}{\partial x^2} + (k_f c_A - k_b c_B)\delta(x))\,dx$$

$$0 = D_B \frac{\partial c_B}{\partial x}|_{x=0} + k_f c_A|_{x=0} - k_b c_B|_{x=0} \tag{14b}$$

These are Butler–Volmer boundary conditions. Apparently, adjusting the boundary conditions at $x = 0$ (the electrode surface) can reproduce Butler–Volmer dynamics entirely and with more generality, giving us another view of electrochemical dynamics. Note that with the diffusion equations in eqs 12a and 12b, we find that the units of k_f and k_b are cm/s, not s^{-1}.

2.1.2.2. Including Reactions Far from the Surface. Before proceeding further, one more point is now appropriate. The differential equation modeling electron transfer (eqs 12a and 12b) can be modified easily to include pre- and post-reactions. For the series of chemical reactions

$$A + e \underset{k_b}{\overset{k_f}{\rightleftharpoons}} B$$

$$B \xrightarrow{k_r} Z$$

where Z is an electronically inactive species, the differential equation in eqs 12a and 12b simply becomes

$$\frac{\partial c_A}{\partial t} = D_A^x \frac{\partial^2 c_A}{\partial x^2} - (k_f c_A - k_b c_B)\delta(x) \tag{15a}$$

$$\frac{\partial c_B}{\partial t} = D_B^x \frac{\partial^2 c_B}{\partial x^2} + (k_f c_A - k_b c_B)\delta(x) - k_r c_B \tag{15b}$$

In this case, k_f and k_b have different units from k_r; the rate constants k_f and k_b have units of cm/s and k_r has units of s^{-1}. Note that the delta function $\delta(x)$ from eqs 12a, 12b, 15a, and 15b has units of cm^{-1}.

2.1.3. Ramp Speed and Measuring Current. To model a linear sweep voltammetry or a cyclic voltammetry experiment, one must propagate the diffusion equations forward in time, while also changing the potential ($\Delta G(t)$ in eqs 6a, 6b, 11a, and 11b). For our purposes, we will imagine that the potential is ramped according to the following equation

$$\Delta G(t) = \Delta G_i + \nu t \tag{16}$$

where ν is the scan rate and ΔG_i is the starting potential. For the cyclic voltammetry experiments, once $\Delta G(t) = \Delta G_f = -\Delta G_i$ the scan is reversed and carried out until $\Delta G(t) = \Delta G_i$. Current in these experiments can be calculated in at least two equivalent ways

$$I(t) = n\mathcal{F}AD_A^x \frac{\partial c(t)}{\partial x}|_{x=0} \tag{17a}$$

or

$$I(t) = n\mathcal{F}A(k_f(t)c_A(t) - k_b(t)c_B(t))|_{x=0} \tag{17b}$$

Here, $\mathcal{F}$ is the Faraday constant, A is the area of the electrode surface, and n is the number of electrons transferred in the electron transfer. For simplicity, we set $n\mathcal{F}A = 1$.

2.2. Electrochemical Dynamics in Two Dimensions. *2.2.1. SH in 2D: Explicitly Modeling ET through a Solvent Reorganization Coordinate.* As described above, simple Butler–Volmer kinetics models electrochemical ET effectively through one parameter α; thus, the kinetics implicitly assumes that ET dynamics is dictated by a slow, rate-limiting motion along a generalized diffusion coordinate from the bulk to the surface. Although this approach is often reasonable in solution (for outer sphere ET), it is also true that dynamics is often limited by water reorganization and other solvent effects (as argued originally by Marcus[35]). Thus, one can easily imagine at least two possible reaction coordinates. With this motivation in mind, and having already reviewed the basic theory of one-dimensional electrochemical dynamics for modeling CV experiments, we will now construct a multidimensional problem by including an additional degree of freedom into our Hamiltonian: an effective solvent reorganization coordinate ζ. Mathematically, we choose a Hamiltonian of the form from eqs 9a, 9b, 9c, 9d, and 9e, with $\vec{r} = (x, \zeta)$. For simplicity, we suppose that the PESs for species A and B are quadratic wells, with a nuclear frequency ω, mass m, and centered at ζ_A (ζ_B)

$$U_A(x, \zeta) = \frac{1}{2}m\omega^2(\zeta_A(x) - \zeta)^2 \tag{18a}$$

$$U_B(\zeta) = \frac{1}{2}m\omega^2(\zeta_B - \zeta)^2 + \Delta G \tag{18b}$$

$$E(x, \zeta) = U_B - U_A = \frac{1}{2}m\omega^2(\zeta_B^2 - \zeta_A^2(x) - 2(\zeta_B - \zeta_A(x))\zeta) + \Delta G \tag{18c}$$

where U_A can have an x dependence through the diabat minimum position $\zeta_A(x)$ and ΔG is determined by the external voltage. Note that U_B is always independent of x.

To model the electrochemical dynamics, we discretize our electrochemical system on a 2D grid, and we solve the following differential equations

$$\vec{J}_A = \left(-D_A^x \frac{\partial c_A}{\partial x} + \frac{F_A^x}{\gamma_x}c_A\right)\hat{x} + \left(-D_A^\zeta \frac{\partial c_A}{\partial \zeta} + \frac{F_A^\zeta}{\gamma_\zeta}c_A\right)\hat{\zeta}$$

$$\vec{J}_B = \left(-D_B^x \frac{\partial c_B}{\partial x} + \frac{F_B^x}{\gamma_x}c_B\right)\hat{x} + \left(-D_B^\zeta \frac{\partial c_B}{\partial \zeta} + \frac{F_B^\zeta}{\gamma_\zeta}c_B\right)\hat{\zeta} \tag{19a}$$

DOI: 10.1021/acs.jpcc.9b02068
J. Phys. Chem. C 2019, 123, 13304−13317

$$\frac{\partial c_A}{\partial t} = D_A^x \frac{\partial^2 c_A}{\partial x^2} + D_A^\zeta \frac{\partial^2 c_A}{\partial \zeta^2} - \frac{F_A^x}{\gamma_x}\frac{\partial c_A}{\partial x} - \frac{\partial F_A^x}{\partial x}\frac{c_A}{\gamma_x} - \frac{F_A^\zeta}{\gamma_\zeta}\frac{\partial c_A}{\partial \zeta} - \frac{\partial F_A^\zeta}{\partial \zeta}\frac{c_A}{\gamma_\zeta} - (k_f c_A - k_b c_B)$$

$$\frac{\partial c_B}{\partial t} = D_B^x \frac{\partial^2 c_B}{\partial x^2} + D_B^\zeta \frac{\partial^2 c_B}{\partial \zeta^2} - \frac{F_B^x}{\gamma_x}\frac{\partial c_B}{\partial x} - \frac{\partial F_B^x}{\partial x}\frac{c_B}{\gamma_x} - \frac{F_B^\zeta}{\gamma_\zeta}\frac{\partial c_B}{\partial \zeta} - \frac{\partial F_B^\zeta}{\partial \zeta}\frac{c_B}{\gamma_\zeta} + (k_f c_A - k_b c_B) \quad (19b)$$

$$c_A(t, x = -1, \zeta) = c_A(t, x = 0, \zeta)$$
$$c_B(t, x = -1, \zeta) = c_B(t, x = 0, \zeta) \quad (19c)$$

D^x, D^ζ are diffusion coefficients in the x and ζ directions, respectively, γ_x, γ_ζ are friction coefficients in the x and ζ directions, respectively ($\gamma_x = \frac{kT}{D^x}$, $\gamma_\zeta = \frac{kT}{D^\zeta}$), and F^x, F^ζ are the mean forces acting on a given species in the x and ζ directions, respectively. From eqs 18a and 18b, the relevant forces are

$$F_A^\zeta(x, \zeta) = m\omega^2(\zeta_A(x) - \zeta) \quad (20a)$$

$$F_A^x(x, \zeta) = -m\omega^2(\zeta_A(x) - \zeta)\frac{d\zeta_A}{dx} \quad (20b)$$

$$F_B^\zeta(\zeta) = m\omega^2(\zeta_B - \zeta) \quad (20c)$$

$$F_B^x(\zeta) = 0 \quad (20d)$$

To visualize the effect of ΔG on the PESs, see Figure 1. The addition of the ζ coordinate allows us to model the electron

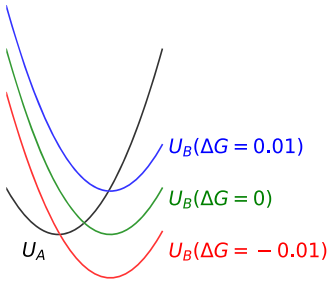


Figure 1. Illustration of the vertical shift in energy that occurs when changing the external voltage, and subsequently ΔG, on the PES U_B from eq 18b.

transfer in the form of "hops" between the species, represented by hopping rates k_f and k_b. These hopping rates depend on the coordinate ζ and are given by

$$k_f(x, \zeta) = \frac{\Gamma(x)}{\hbar} f(E(x, \zeta)) \quad (21a)$$

$$k_b(x, \zeta) = \frac{\Gamma(x)}{\hbar}(1 - f(E(x, \zeta))) \quad (21b)$$

$$\Gamma(x) = \Gamma_0 \delta(x) \quad (21c)$$

where $\Gamma(x)$ is the function that represents the strength of the electrode−molecule coupling and $f(E) = \frac{1}{1 + e^{\beta E}}$ is the fermi function.

The system is governed by the following initial conditions

$$c_A(t = 0, x, \zeta) = \frac{e^{-\beta U_A(x,\zeta)}}{\int d\zeta e^{-\beta U_A(x,\zeta)}} \quad (22a)$$

$$c_B(t = 0, x, \zeta) = 0 \quad (22b)$$

and boundary conditions

$$c_A(t, x = \infty, \zeta) = \frac{e^{-\beta U_A(x,\zeta)}}{\int d\zeta e^{-\beta U_A(x,\zeta)}} \quad (23a)$$

$$c_B(t, x = \infty, \zeta) = 0 \quad (23b)$$

$$c_A(t, x, \zeta = \pm\infty) = c_B(t, x, \zeta = \pm\infty) = 0 \quad (23c)$$

The initial conditions in eqs 22a and 22b enforce the fact that only A is present initially and at a uniform concentration everywhere in the x-direction; furthermore, there is a Boltzmann distribution in the ζ direction. The boundary conditions in eqs 23a, 23b, and 23c enforce the fact that there is no concentration of either species at the boundaries of the ζ coordinate ($\zeta \to \pm\infty$), and that the concentrations of A and B are equal to their initial concentrations infinitely far from the electrode in the x-direction ($x \to \infty$). For simplicity, we fix the diffusion constant to be constant and equal for both species A and B ($D_A^x = D_B^x = D_A^\zeta = D_B^\zeta$).

2.2.2. Nuances of Broadening: a Broadened Classical Master Equation (BCME). In cases where the metal molecule coupling Γ is larger than kT, level broadening becomes important: for molecules chemisorbed or physisorbed on surfaces, electrons are shared in an adiabatic state quantum mechanically between molecule and surface, and the electronic motion is not simply hopping back and forth. To capture the more complex hybridized dynamics that arises from the continuum of electronic states in the metal, a reasonable fix is to modify our diabatic forces as follows[36]

$$F_A^{x,\mathrm{broad}}(x, \zeta) = -m\omega^2(\zeta_A(x) - \zeta)\frac{d\zeta_A}{dx} - \frac{dE}{dx}(n(E(x, \zeta)) - f(E(x, \zeta))) \quad (24a)$$

$$F_A^{\zeta,\mathrm{broad}}(x, \zeta) = m\omega^2(\zeta_A(x) - \zeta) - \frac{dE}{d\zeta}(n(E(x, \zeta)) - f(E(x, \zeta))) \quad (24b)$$

$$F_B^{x,\mathrm{broad}}(x, \zeta) = -\frac{dE}{dx}(n(E(x, \zeta)) - f(E(x, \zeta))) \quad (24c)$$

$$F_B^{\zeta,\mathrm{broad}}(x, \zeta) = m\omega^2(\zeta_B - \zeta) - \frac{dE}{d\zeta}(n(E(x, \zeta)) - f(E(x, \zeta))) \quad (24d)$$

Here, $n(E)$ is the broadened population and W is the electronic bandwidth

$$n(E) = \int_{-W}^{W} \frac{d\epsilon}{2\pi} \frac{\Gamma}{(\epsilon - E)^2 + \frac{\Gamma^2}{4}} f(\epsilon) \quad (25)$$

chosen such that $W \gg \Gamma$. To visualize the surfaces from eqs 18a, 18b, 24a, 24b, 24c, and 24d, see Figure 2, and to visualize the 2D surfaces, see Figure 3.

DOI: 10.1021/acs.jpcc.9b02068
J. Phys. Chem. C 2019, 123, 13304−13317

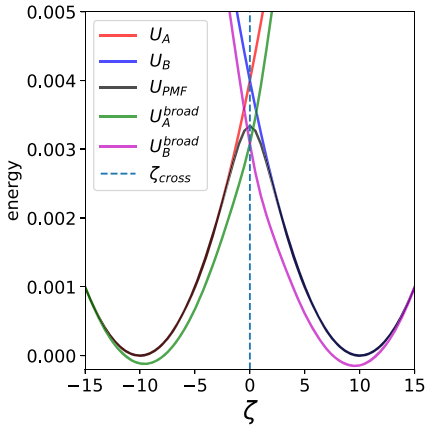


Figure 2. Potential energy surfaces as a function of the solvent reorganization coordinate ζ, unbroadened (U_A and U_B) and broadened (U_A^{broad} and U_B^{broad}), and potentials of mean force (U_{PMF}), for diabats in eqs 18a, 18b, 18c, 29a, and 29b, with m = 2000, ω = 0.0002, $\zeta_A = -10$, $\zeta_B = 10$, Γ = 0.002, and $\Delta G = 0$. All parameters are in atomic units (au).

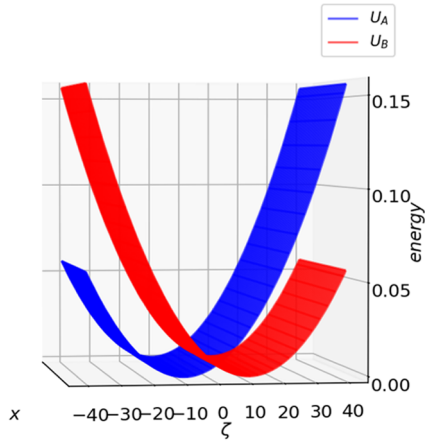


Figure 3. Potential energy surfaces as a function of the diffusion coordinate x and solvent reorganization coordinate ζ, with m = 2000, ω = 0.00025, $\zeta_A = -10$, $\zeta_B = 10$, $\Gamma = 10^{-6}$, and $\Delta G = 0$. All parameters are in atomic units (au).

2.2.3. Measuring Current in 2D. For all calculations, where we explicitly model ζ, one can calculate current in two different ways

$$I(t) = n\mathcal{F}AD_A^x \int_{\zeta_i}^{\zeta_f} d\zeta \frac{\partial c_A(t,\zeta_i)}{\partial x}|_{x=0}$$

$$I(t) \approx n\mathcal{F}AD_A^x \sum_i^{N_\zeta} d\zeta \frac{\partial c_A(t,\zeta_i)}{\partial x}|_{x=0} \quad (26a)$$

or

$$I(t) = n\mathcal{F}A \int_{\zeta_i}^{\zeta_f} d\zeta (k_f(t,\zeta_i)c_A(t,\zeta_i) - k_b(t,\zeta_i)c_B(t,\zeta_i))|_{x=0}$$

$$I(t) \approx n\mathcal{F}A \sum_i^{N_\zeta} d\zeta (k_f(t,\zeta_i)c_A(t,\zeta_i) - k_b(t,\zeta_i)c_B(t,\zeta_i))|_{x=0} \quad (26b)$$

2.2.4. Coarse Graining and Marginalizing Out ζ: The 1D Marcus−Hush (MH) Model. Equations 19a, 19b, and 19c represent a general approach to modeling electrochemical ET, and yet one often seeks the simplest possible approach. To that end, one often seeks to marginalize out the reorganization coordinate direction, leading to the following marginal probability distribution $c(x, t)$

$$\overrightarrow{J_A} = -D_A^x \frac{\partial c_A}{\partial x}\hat{x}$$

$$\overrightarrow{J_B} = -D_B^x \frac{\partial c_B}{\partial x}\hat{x} \quad (27a)$$

$$\frac{\partial c_A}{\partial t} = -\vec{\nabla}\cdot\overrightarrow{J_A} - (\widetilde{k_f}c_A - \widetilde{k_b}c_B)\delta(x)$$

$$= D_A^x \frac{\partial^2 c_A}{\partial x^2} - (\widetilde{k_f}c_A - \widetilde{k_b}c_B)\delta(x)$$

$$\frac{\partial c_B}{\partial t} = -\vec{\nabla}\cdot\overrightarrow{J_B} + (\widetilde{k_f}c_A - \widetilde{k_b}c_B)\delta(x)$$

$$= D_B^x \frac{\partial^2 c_B}{\partial x^2} + (\widetilde{k_f}c_A - \widetilde{k_b}c_B)\delta(x) \quad (27b)$$

Obviously, eqs 27a and 27b are equivalent to eqs 12a and 12b; although in this case, the motion in the ζ direction gives a new average hopping rate, $\tilde{k}_{f/b}$

$$\widetilde{k_f} = \frac{\Gamma_0}{\hbar}\frac{\int_{-\infty}^{\infty} d\zeta\ e^{-\beta U_A(0,\zeta)} f(E(0,\zeta))}{\int_{-\infty}^{\infty} d\zeta\ e^{-\beta U_A(0,\zeta)}} \quad (28a)$$

$$\widetilde{k_b} = \frac{\Gamma_0}{\hbar}\frac{\int_{-\infty}^{\infty} d\zeta\ e^{-\beta U_B(\zeta)}(1-f(E(0,\zeta)))}{\int_{-\infty}^{\infty} d\zeta\ e^{-\beta U_B(\zeta)}} \quad (28b)$$

The rates $\widetilde{k_f}$, $\widetilde{k_b}$ are just the original hopping rates weighted by the Boltzmann average of being at a given position in ζ at x = 0. Equations 28a and 28b arise from the assumption that the equilibration in ζ is fast relative to other time scales in the simulation. For the Hamiltonian in eqs 9a, 9b, 9c, 9d, and 9e with roughly equal diffusion in x and ζ, the relevant condition for fast nuclear equilibration relative to the time scale of the driving force is $\frac{m\omega^2}{\gamma} = \frac{Dm\omega^2}{kT} > \frac{\nu}{kT}$. This condition states that the time required to change the driving force by kT should be larger than the relaxation time of a damped harmonic oscillator (which in the overdamped limit is $\frac{m\omega^2}{\gamma}$). This condition should be satisfied for almost all experiments.

The implementation of $\tilde{k}_f$ and $\tilde{k}_b$ as the rate constants for Butler−Volmer dynamics in eq 5 in lieu of the rate constants in eqs 6a and 6b is known in the electrochemical literature as the Marcus−Hush (MH) boundary conditions.[37] Obviously, eqs 28a and 28b are equivalent to the Marcus electrochemical rate constants; in this paper, even though we are in the slightly overdamped regime, the Zusman corrections (for solvent overdamping effects on the rate constant) should be small and will not be considered. Below, we will refer to the utilization of the rate constants $\tilde{k}_f$ and $\tilde{k}_b$ in the SH framework as a 1D MH model. Note that if Γ is larger than kT, then the potentials U_A and U_B (within the BCME approximation) in the above equations need to be replaced with the broadened PESs

DOI: 10.1021/acs.jpcc.9b02068
J. Phys. Chem. C 2019, 123, 13304−13317

$$U_A^{broad}(0,\zeta) = \frac{1}{2}m\omega^2(\zeta_A(0)-\zeta)^2 + \int_{\zeta_0}^{\zeta} d\zeta'(n(E(0,\zeta'))-f(E(0,\zeta')))\frac{dE}{d\zeta'} \quad (29a)$$

$$U_B^{broad}(0,\zeta) = \frac{1}{2}m\omega^2(\zeta_B-\zeta)^2 + \Delta G + \int_{\zeta_0}^{\zeta} d\zeta'(n(E(0,\zeta'))-f(E(0,\zeta')))\frac{dE}{d\zeta'} \quad (29b)$$

2.3. Alternative to Solving Ordinary Differential Equation (ODE): Diagonalizing the Fokker−Planck Operator. The simplest means to propagate the electrochemical dynamics in eqs 12a, 12b, 19a, 19b, 19c, 27a, and 27b is to use an implicit ordinary differential equation (ODE) solver. Note that an implicit ODE solver is necessary, because a more conventional explicit ODE solver (e.g., RK4[38]) is unstable for this purpose. The root of the problem is the stiff behavior of these ODEs;[39] for the 1D data in the Results and Discussion, we have chosen to use the real-valued variable-coefficient ordinary differential equation ("vode") solver with the backward difference formula method.[40]

As an alternative to vode, there is another approach, namely, one can cast $\frac{\partial c_A}{\partial t}$ $\left(\frac{\partial c_B}{\partial t}\right)$ as a matrix equation and diagonalize the corresponding matrix operator to obtain an exact answer for the time evolution of c_A (c_B)[c]. The diagonalization of this "Fokker−Planck" operator has been previously applied to study ET dynamics in a two-state system with diffusion.[41] For our purposes, eqs 12a and 12b can be written in the following way

$$\frac{\partial c_A}{\partial t} = \mathcal{L}_A^x c_A - (k_f c_A - k_b c_B)\delta(x) \quad (30a)$$

$$\frac{\partial c_B}{\partial t} = \mathcal{L}_B^x c_B + (k_f c_A - k_b c_B)\delta(x) \quad (30b)$$

Here, we define superoperators

$$\mathcal{L}_A^x = \frac{\partial}{\partial x}\left(D_A^x\frac{\partial}{\partial x} - \frac{F_A^x}{\gamma_x}\right) \quad (31a)$$

$$\mathcal{L}_B^x = \frac{\partial}{\partial x}\left(D_B^x\frac{\partial}{\partial x} - \frac{F_B^x}{\gamma_x}\right) \quad (31b)$$

and we allow for a drift term $\frac{F^x}{\gamma_x}$ for generality; note that for the case of eq 12a, $F^x \equiv 0$. Similarly, eq 19a can be written as

$$\frac{\partial c_A}{\partial t} = (\mathcal{L}_A^x + \mathcal{L}_A^\zeta)c_A - (k_f c_A - k_b c_B)\delta(x) \quad (32a)$$

$$\frac{\partial c_B}{\partial t} = (\mathcal{L}_B^x + \mathcal{L}_B^\zeta)c_B + (k_f c_A - k_b c_B)\delta(x) \quad (32b)$$

$$\mathcal{L}_A^\zeta = \frac{\partial}{\partial \zeta}\left(D_A^\zeta\frac{\partial}{\partial \zeta} - \frac{F_A^\zeta}{\gamma_\zeta}\right) \quad (32c)$$

$$\mathcal{L}_B^\zeta = \frac{\partial}{\partial \zeta}\left(D_B^\zeta\frac{\partial}{\partial \zeta} - \frac{F_B^\zeta}{\gamma_\zeta}\right) \quad (32d)$$

By combining $\mathcal{L}_A^x$, $\mathcal{L}_B^x$, $\mathcal{L}_A^\zeta$, $\mathcal{L}_B^\zeta$, k_f, and k_b, we obtain the general matrix equation for both c_A and c_B

$$\begin{pmatrix}\dot{c}_A\\ \dot{c}_B\end{pmatrix} = \begin{pmatrix}\mathcal{L}_A - k_f\delta(x) & k_b\delta(x)\\ k_f\delta(x) & \mathcal{L}_B - k_b\delta(x)\end{pmatrix}\begin{pmatrix}c_A\\ c_B\end{pmatrix} + \vec{y}$$

$$\dot{\vec{c}} = \mathcal{M}\vec{c} + \vec{y} \quad (33)$$

where $\mathcal{L}_A = \mathcal{L}_A^x$ $(\mathcal{L}_B = \mathcal{L}_B^x)$ in the 1D model and $\mathcal{L}_A = \mathcal{L}_A^x + \mathcal{L}_A^\zeta$ $(\mathcal{L}_B = \mathcal{L}_B^x + \mathcal{L}_B^\zeta)$ in the 2D model. Here, the term $\vec{y}$ is used to include the bath conditions from eqs 13a, 13b, 13c, 13d, 23a, 23b, and 23c, which maintain a static condition at the bath boundary, i.e., $\dot{\vec{c}}(x=\infty) = \vec{0}$. In other words, $\vec{y}(x\neq\infty) = 0$ and $\vec{y}(x=\infty) = -(\mathcal{M}\vec{c})(x=\infty)$.

Obviously, $\mathcal{M}$ is in general non-Hermitian, given that (i) $\mathcal{L}_A$ $(\mathcal{L}_B)$ is non-Hermitian if there is a potential U_A (U_B) and (ii) the off-diagonal elements of $\mathcal{M}$ are not equal $(k_f \neq k_b)$ unless $E = 0$. Since the diagonalization of non-Hermitian matrices is often unstable, one would like to transform $\mathcal{M}$ into a Hermitian matrix. To do so, there is a common method[42] for converting the non-Hermitian operator $\tilde{\mathcal{L}}_A$ $(\tilde{\mathcal{L}}_B)$

$$\tilde{\mathcal{L}}_A = e^{\beta U_A/2}\mathcal{L}_A e^{-\beta U_A/2} \quad (34a)$$

$$\tilde{\mathcal{L}}_B = e^{\beta U_B/2}\mathcal{L}_B e^{-\beta U_B/2} \quad (34b)$$

With the above transformation of $\mathcal{L}_A$ $(\mathcal{L}_B)$ in mind, we can define a similarity transformation matrix S as

$$S = \begin{pmatrix}e^{\beta U_A/2} & 0\\ 0 & e^{\beta U_B/2}\end{pmatrix} \quad (35)$$

such that the new operator $\tilde{\mathcal{M}}$

$$\tilde{\mathcal{M}} = S\mathcal{M}S^{-1} = \begin{pmatrix}\tilde{\mathcal{L}}_A - k_f\delta(x) & k_b\delta(x)e^{-\beta E/2}\\ k_f\delta(x)e^{\beta E/2} & \tilde{\mathcal{L}}_B - k_b\delta(x)\end{pmatrix} \quad (36)$$

is Hermitian and can be easily diagonalized. Although the eigenvectors of $\tilde{\mathcal{M}}$ will differ from those of $\mathcal{M}$, $\mathcal{M}$ and $\tilde{\mathcal{M}}$ are related by a similarity transformation, so that the eigenvalues are identical for both and one can analyze the dynamics of the system at any arbitrary time. Note that in eq 36 for a 2D simulation, k_f, k_b, and E are functions of the coordinates x and ζ.

Simulating a linear sweep voltammetry experiment can be done with matrix algebra by the diagonalization of $\tilde{\mathcal{M}}$ at each time step (since $\tilde{\mathcal{M}}$ is a function of $\Delta G(t)$), yielding $\tilde{\mathcal{M}} = P\Lambda P^T$. The eigenvalues Λ are always nonpositive, corresponding to decay rates along modes represented by the eigenvectors of P, and for such a dissipative system, there is always one zero eigenvalue corresponding to the equilibrium or steady state[d]. At this point, we can change variables and recast the differential equation for the time evolution of c_A and c_B into renormalized coordinates

$$\vec{b} \equiv P^T S\vec{c} \quad (37a)$$

DOI: 10.1021/acs.jpcc.9b02068
J. Phys. Chem. C 2019, 123, 13304−13317

$$\vec{z} \equiv P^{\mathrm{T}} S \vec{y} \tag{37b}$$

The final equation of motion becomes

$$\dot{\vec{b}} = \Lambda \vec{b} + \vec{z} \tag{37c}$$

Equation 37c can be solved exactly, with the solution for any arbitrary time step given by

$$\vec{b}(t) = \vec{b}_{\mathrm{eq}} + (\vec{b} - \vec{b}_{\mathrm{eq}}) \mathrm{e}^{\Lambda t} \tag{38a}$$

$$\vec{b}_{\mathrm{eq}} = -\Lambda^{-1} \vec{z} \tag{38b}$$

Finally, using eq 37a, we can convert $\vec{b}(t)$ back to $\vec{c}(t) = \begin{pmatrix} c_{\mathrm{A}} \\ c_{\mathrm{B}} \end{pmatrix}$ using P and S: $\vec{c} = S^{-1} P \vec{b}$. Hence, one can easily calculate the current at each time step with complete numerical stability.

2.4. Parameterization. We will work in standard units throughout this paper and, unless stated otherwise, set $\Delta G^{\circ} = 0$ V, $m = 1.82 \times 10^{-27}$ kg (2000 au), $T = 300$ K (0.00095 au), $\zeta_{\mathrm{A}}(x) = \zeta_{\mathrm{A}}^{0} = -5.29$ Å (−10 au), $\zeta_{\mathrm{B}} = 5.29$ Å (10 au), $W = 10^{3} \times \Gamma$, $N_x = 50$, and $N_\zeta = 101$. The size of the grid in x is given by $L_x = 6\sqrt{D^x t_{\mathrm{T}}}$, where t_{T} is the total time of the simulation, defined by the starting and ending ΔG and ν, $t_{\mathrm{T}} = \frac{|\Delta G_{\mathrm{f}} - \Delta G_{\mathrm{i}}|}{\nu}$ for linear sweeps and $t = \frac{2|\Delta G_{\mathrm{f}} - \Delta G_{\mathrm{i}}|}{\nu}$ for cyclic sweeps. The size of the grid in ζ is given by $L_\zeta = 4(\zeta_{\mathrm{B}} - \zeta_{\mathrm{A}})$, with endpoints $[4\zeta_{\mathrm{A}}, 4\zeta_{\mathrm{B}}]$, and the grid spacing in both x and ζ is uniform, such that $\mathrm{d}x = \frac{L_x}{N_x}$ and $\mathrm{d}\zeta = \frac{L_\zeta}{N_\zeta}$. The current values in Figures 5, 6, 7, 8, 10, and 11 are rescaled by a factor of 10^9.

3. RESULTS

We have thus far presented several distinct approaches for simulating electrochemical systems. To better understand these approaches, we will now consider a host of different situations and quantitatively analyze the prediction of each approach. When will different approaches agree? And if they disagree, which approach is appropriate?

3.1. Verification of 1D Model. Our first goal is to numerically demonstrate the equivalence of surface hopping with boundary conditions (eqs 12a, 12b, 13a, 13b, 13c, and 13d) against the Nernstian (eqs 1a, 1b, and 4) and Butler Volmer (eqs 1a, 1b, and 5) approaches. In Figure 4, we plot simulated cyclic voltammograms for two chemical reaction types, with both methods for calculating current (eqs 17a and 17b) and three different dynamics methods, Nernstian (eqs 1a, 1b, and 4), Butler–Volmer (eqs 1a, 1b, and 5), and surface hopping (eqs 12a, 12b, 13a, 13b, 13c, and 13d). In all cases, we see an excellent agreement between the surface hopping dynamics and the standard Nernstian and Butler–Volmer approaches whichever way the current is calculated.

In addition to the case of a symmetric barrier between oxidation and reduction, the surface hopping method can also handle the case of an asymmetric barrier, $\alpha \neq 0.5$[e]. In Figure 5, we plot results for the same models and parameterizations as in Figure 4, but with $\alpha = 0.2$. Obviously, we do not expect Nernstian dynamics to recover the correct current due to the asymmetric barrier, but we do see quantitative agreement between the hopping approach and Butler–Volmer kinetics, providing an additional validation for the hopping approach.

3.2. Cases where 2D and 1D MH Model Agree. Next, we examine situations under which the 1D MH model can recover the same result as that of the full 2D model. Plotted in Figures 6 and 7 are linear sweep voltammograms for cases where the 1D MH model agrees with the 2D model, for four different coupling strengths and two different reorganization energies. In the case of moderate reorganization energies (Figure 6), all three methods (1D, 1D MH, and 2D) give the same results for large enough Γ, but as λ_0 increases, the agreement between the 1D model and the 1D MH/2D model decreases (Figure 7).

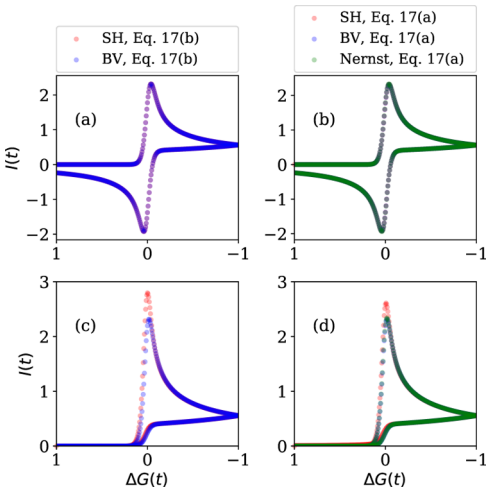


Figure 4. 1D cyclic voltammograms (CV) for the reaction $\mathrm{A} + \mathrm{e}^{-} \underset{k_{\mathrm{b}}}{\overset{k_{\mathrm{f}}}{\rightleftharpoons}} \mathrm{B}$, both with ((c) and (d)) and without ((a) and (b)) the postreaction $\mathrm{B} \xrightarrow{k} \mathrm{Z}$. (a) CV measuring current by the difference in forward and backward rates, without the postreaction $\mathrm{B} \xrightarrow{k} \mathrm{Z}$. (b) CV measuring current by the flux of A at the electrode, without the postreaction $\mathrm{B} \xrightarrow{k} \mathrm{Z}$. (c) CV measuring current by the difference in forward and backward rates, with the postreaction $\mathrm{B} \xrightarrow{k} \mathrm{Z}$. (d) CV measuring current by the flux of A at the electrode, with the postreaction $\mathrm{B} \xrightarrow{k} \mathrm{Z}$. Note that k_{f} and k_{b} are not explicitly modeled when using Nernst boundary conditions, preventing the use of the difference in forward and backward rates as a measure of the current. Parameters are set to $D^x = 1$ cm^2/s, $\nu = 1$ V/s, $\Delta G_{\mathrm{i}} = 1$ V, $\Delta G_{\mathrm{f}} = -1$ V, $N_x = 200$, $k = 100$ s^{-1}, $k^{\circ} = 1000$ cm/s, $\alpha = 0.5$. We see a quantitative agreement between the surface hopping dynamics and both Nernstian and Butler–Volmer dynamics, suggesting that all of the approaches are applicable for simulating these systems.

The regime under which the 1D, the 1D MH, and 2D models all agree can be considered the case where the dynamics is mass transfer limited, i.e., the dynamics along the x coordinate is rate limiting. By contrast, the high reorganization energy/low coupling regime can be understood as the case where the dynamics is limited by the motion along the solvent reorganization coordinate ζ. Nevertheless, from the fact that the 1D MH model always recaptures the 2D results, it appears that the 1D MH model may be adequate for capturing the dynamics of electrochemical systems in all cases. And yet, there should be instances where the average hopping rate of the 1D MH model should not be adequate for modeling the full dynamics of the 2D system. Let us now address this hypothesis.

3.3. Cases where 2D and 1D MH do not Agree. To construct a situation where the 1D MH and 2D models differ, let us choose nonseparable PESs, where ζ and x are entangled. Since the 1D MH model simulates dynamics only in x, we

DOI: 10.1021/acs.jpcc.9b02068
J. Phys. Chem. C 2019, 123, 13304−13317

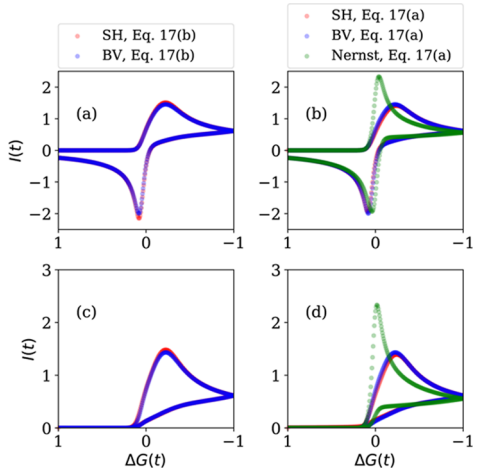


Figure 5. 1D cyclic voltammograms (CV) for the same conditions as in Figure 1 but with an asymmetric barrier between oxidation and reduction, given by $\alpha = 0.2$. Parameters are set to $D^x = 1$ cm^2/s, $\nu = 1$ V/s, $\Delta G_i = 1$ V, $\Delta G_f = -1$ V, $N_x = 200$, $k = 100$ s^{-1}, $k^\circ = 1$ cm/s, $\alpha = 0.2$. Note that k° is decreased relative to the symmetric case; if the kinetics are very facile, as evinced by a large k°, then the asymmetry of the barrier will have no effect on the dynamics. Similarly to the $\alpha = 0.5$ case, we see a quantitative agreement between the hopping approach and the Butler–Volmer approach. Note that the Nernstian dynamics cannot recover the correct answer, since we have introduced an asymmetric barrier and relatively slow ET kinetics in this case.

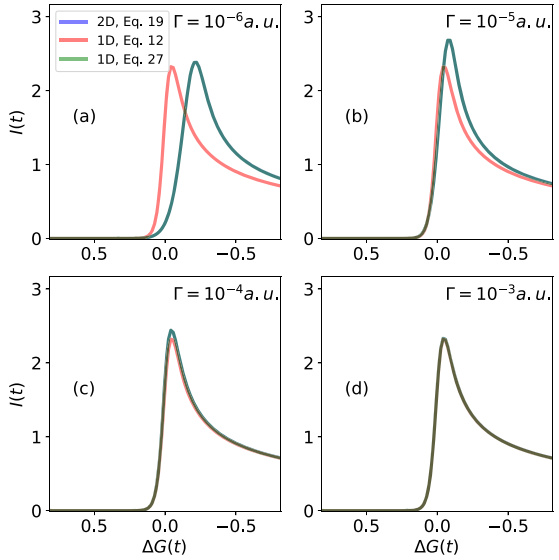


Figure 6. Linear sweep voltammograms for simulations where the 1D MH model (eqs 27a and 27b) and full 2D model (eqs 19a, 19b, and 19c) agree, with an intermediate reorganization energy. $\Delta G_i = 0.816$ V, $\Delta G_f = -0.816$ V, $D = 5.5 \times 10^{-4}$ cm^2/s, $\omega = 1.03 \times 10^{13}$ s^{-1}, $\lambda_0 = 26.32\ kT$, and $\nu = 112$ V/s for each subplot. (a) $\frac{\Gamma}{\hbar} = 1.40 \times 10^7$ cm/s, (b) $\frac{\Gamma}{\hbar} = 1.40 \times 10^8$ cm/s, (c) $\frac{\Gamma}{\hbar} = 1.40 \times 10^9$ cm/s, (d) $\frac{\Gamma}{\hbar} = 1.40 \times 10^{10}$ cm/s. These plots suggest that utilizing the 1D MH model in lieu of the 2D model is appropriate regardless of the coupling strength for moderate reorganization energies; although at lower coupling strengths, the regular 1D model (eqs 12a and 12b) fails and does not agree with the 2D model. Note that the green and blue traces representing the 1D MH and 2D models, respectively, seem indistinguishable due to the quantitative agreement between the two methods.

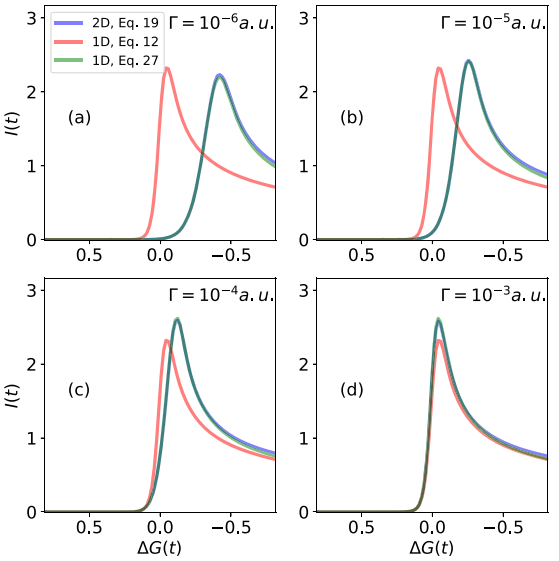


Figure 7. Linear sweep voltammograms for simulations where the 1D MH model (eqs 27a and 27b) and full 2D model (eqs 19a, 19b, and 19c) agree, with a moderately large reorganization energy. $\Delta G_i = 0.816$ V, $\Delta G_f = -0.816$ V, $D = 5.5 \times 10^{-4}$ cm^2/s, $\omega = 1.24 \times 10^{13}$ s^{-1}, $\lambda_0 = 37.89\ kT$, and $\nu = 112$ V/s for each subplot. (a) $\frac{\Gamma}{\hbar} = 1.40 \times 10^7$ cm/s, (b) $\frac{\Gamma}{\hbar} = 1.40 \times 10^8$ cm/s, (c) $\frac{\Gamma}{\hbar} = 1.40 \times 10^9$ cm/s, (d) $\frac{\Gamma}{\hbar} = 1.40 \times 10^{10}$ cm/s. These plots suggest that utilizing the 1D MH model in lieu of the 2D model is appropriate regardless of coupling strength for large reorganization energies. Again, as in Figure 6, the regular 1D model is valid only when the coupling strength is large $\left(\frac{\Gamma}{\hbar} > \omega\right)$.

suspect that the entanglement of x and ζ should give rise to different results compared to the 2D model. To do this, instead of using $\zeta_A(x) = \zeta_A^0$ (in eq 18b) as a constant value, we choose the functional form

$$\zeta_A(x) = (\zeta_A^0 - \zeta_A^\infty)e^{-\sigma x^2} + \zeta_A^\infty,\ \sigma \gg \frac{1}{(dx)^2} \tag{39}$$

This creates a situation where the diabat well minimum for species A takes on the value ζ_A^0 at $x = 0$ and the value ζ_A^∞ for all other x. The switch off occurs over a length scale much smaller than the grid spacing dx. Consider now a situation where $\zeta_A^\infty = -5.29$ Å for all x values except at the electrode surface. When species A approaches the metal from $x > 0$, necessarily there must be an additional relaxation as the solute concentration c_A adjusts to the new surface at $x = 0$. Moreover, this adjustment cannot be measured by a simple difference in the reorganization energy at $x = 0$. In such cases, the solute concentrations c_A and c_B need not relax faster than the time scales k_f and k_b.

Plotted in Figures 8 and 9 are linear sweep voltammograms for different ζ_A positions at $x = 0$ for four different coupling strengths. Although the difference between the 1D MH and 2D models is modest in Figure 8 ($\zeta_A(x = 0) = -5.82$ Å), the difference becomes readily apparent in Figure 9 ($\zeta_A(x = 0) = -6.35$ Å). Effectively, we find that the 1D MH model is adequate for situations where the two dimensions are separable, but the 1D MH model fails when separability is no longer guaranteed. Now, one may well question whether the data in Figures 8 and 9 is anomalous and caused by a discontinuous PES. To that end, in Appendix B, we study

DOI: 10.1021/acs.jpcc.9b02068
J. Phys. Chem. C 2019, 123, 13304−13317

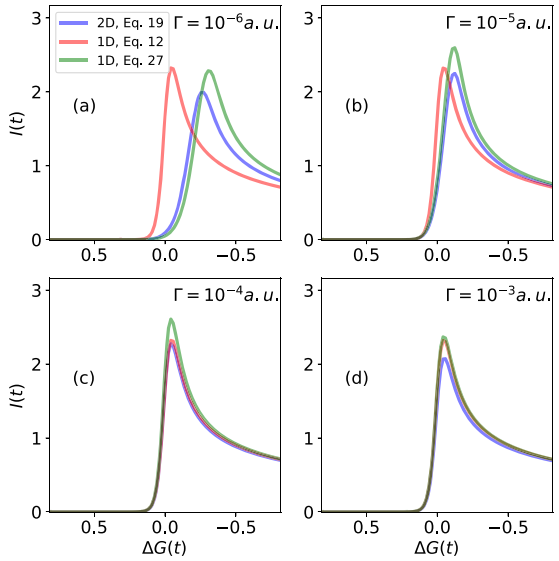


Figure 8. Linear sweep voltammograms for simulations where the 1D MH model (eqs 27a and 27b) and full 2D model (eqs 19a, 19b, and 19c) do not agree, with $\zeta_A^0 = -5.82$ Å and $\zeta_A^\infty = -5.29$ Å in eq 39. $\Delta G_i = 0.816$ V, $\Delta G_f = -0.816$ V, $\sigma = \frac{10}{dx^2}$, $D = 5.5 \times 10^{-4}$ cm^2/s, $\omega = 1.03 \times 10^{13}$ s^{-1}, $\lambda_0 = 29.01$ kT, and $\nu = 112$ V/s for each subplot. (a) $\frac{\Gamma}{\hbar} = 1.40 \times 10^7$ cm/s, (b) $\frac{\Gamma}{\hbar} = 1.40 \times 10^8$ cm/s, (c) $\frac{\Gamma}{\hbar} = 1.40 \times 10^9$ cm/s, (d) $\frac{\Gamma}{\hbar} = 1.40 \times 10^{10}$ cm/s. By shifting ζ_A in the 2D model, and breaking separability of x and ζ in the Hamiltonian, we see that the 1D MH and 2D models can yield somewhat different results.

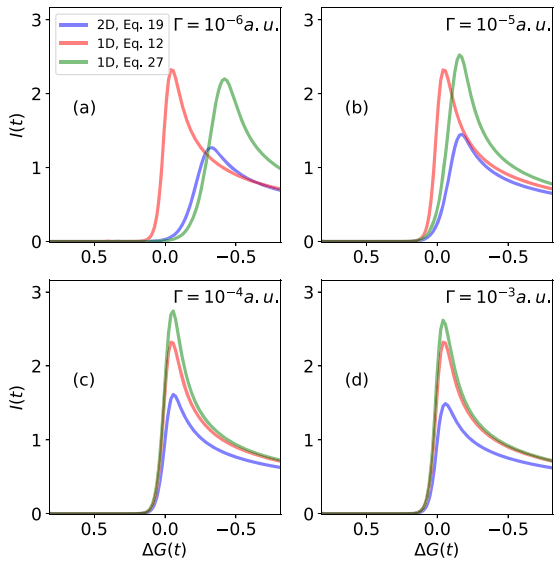


Figure 9. Linear sweep voltammograms for simulations where the 1D MH model (eqs 27a and 27b) and full 2D model (eqs 19a, 19b, and 19c) do not agree at all, with $\zeta_A^0 = -6.35$ Å and $\zeta_A^\infty = -5.29$ Å in eq 39. $\Delta G_i = 0.816$ V, $\Delta G_f = -0.816$ V, $\sigma = \frac{10}{dx^2}$, $D = 5.5 \times 10^{-4}$ cm^2/s, $\omega = 1.03 \times 10^{13}$ s^{-1}, $\lambda_0 = 31.84$ kT, and $\nu = 112$ V/s for each subplot. (a) $\frac{\Gamma}{\hbar} = 1.40 \times 10^7$ cm/s, (b) $\frac{\Gamma}{\hbar} = 1.40 \times 10^8$ cm/s, (c) $\frac{\Gamma}{\hbar} = 1.40 \times 10^9$ cm/s, (d) $\frac{\Gamma}{\hbar} = 1.40 \times 10^{10}$ cm/s. By shifting ζ_A even more at $x = 0$, we see a complete breakdown of the 1D MH model as far as replicating the 2D model results.

smaller σ values for $\zeta_A(x)$ and investigate model Hamiltonians that smoothly bridge the gap between separable and inseparable. We find that even with smooth PESs, the 1D MH model still fails without separability. In the future, understanding the nature of the PESs and the separability of the diffusion and solvent reorganization coordinates will be essential: after all, the reorganization energy for an ion must depend strongly on the proximity to the metal surface.

4. DISCUSSION

4.1. Electrostatic Interactions. At this point, we have shown that in many cases, 1D simulations of electrochemical voltammetry experiments are appropriate, unless there is a significant nonseparability between the diffusion and solvent reorganization coordinates. That being said, there is still one additional important consideration that all of the simulations in this work do not account for: electrostatic interactions between charged particles (redox species and/or electrolyte ions). These effects can have a measurable effect on the dynamics and subsequent $I-V$ curve for a given simulation. The importance of accounting for these interactions can be ascertained by investigating the concentrations and current profile in a simulation that is allowed to run for long times after reaching the final voltage in a linear sweep experiment.

To that end, consider Figure 10, where dx is fixed, but we choose a different number of grid points. We present 1D linear sweep voltammograms using the surface hopping approach.

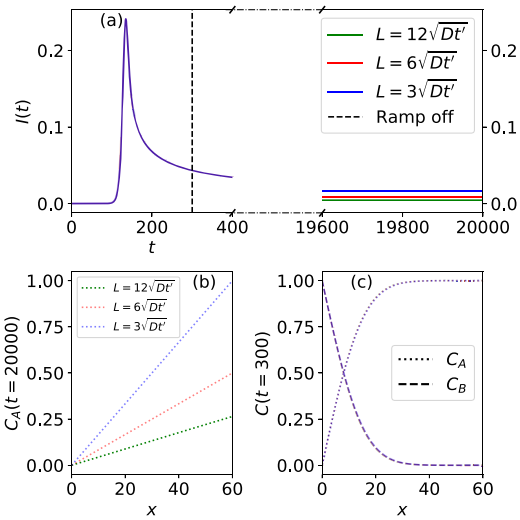


Figure 10. Linear sweep voltammogram and concentration profile for a simulation that is allowed to run for long times after completing the sweep, for different length grids ($x_f - x_0$). $D = 1$, $\nu = 0.01$, and $t' = 300$. t' is the time at which the potential ramp is turned off. (a) Linear sweep voltammograms for the case where the simulation grid length is set to $12\sqrt{Dt'}$, $6\sqrt{Dt'}$ and $3\sqrt{Dt'}$. The dotted line is the point at which the potential is no longer ramped and held at that value for the remainder of the simulation. (b) Concentration profiles for A at the end of the simulation, from $x = 0$ to $x = 3\sqrt{Dt'}$. (c) Concentration profiles for A and B at the time at which the potential ramp is turned off, from $x = 0$ to $x = 3\sqrt{Dt'}$. At short times all three grid spacings provide the same concentration and current profile, but at long times begin to diverge. The effect of grid length on the outcome of these steady-state simulations suggests that accurate modeling of electrostatic interactions between particles is necessary for a complete understanding of the dynamics of these systems at long times.

DOI: 10.1021/acs.jpcc.9b02068
J. Phys. Chem. C 2019, 123, 13304−13317

We find that at long times, the concentration profiles of c_A and c_B differ greatly as a function of the length of the 1D-grid, which is also detectable through a slight difference in the steady-state current between the simulations. In fact, a simple analysis shows that the steady-state current using eq 17a is

$$I_{ss} = n\mathcal{F}AD_A^x \frac{\partial c_A^{ss}}{\partial x}|_{x=0}$$

$$I_{ss} = n\mathcal{F}AD_A^x \frac{c_A^{ss}(x = dx) - c_A^0}{dx} \quad (40)$$

where c_A^0 is the steady-state concentration of A at the electrode surface, whose ratio is almost (but not exactly) equal to the ratio of backward and forward hopping rates

$$\frac{c_A^0}{c_B^0} = \frac{k_b}{k_f} + \kappa = e^{\beta\Delta G} + \kappa \quad (41)$$

where κ is a small number representing the deviation of the steady-state concentrations at the electrode surface from the Nernstian value.

To develop an analytical expression for I_{ss}, we note that since the diffusion constants of both A and B are equal, the fluxes of A and B are equal and that $c_A + c_B = c_A^{bulk} + c_B^{bulk}$ everywhere in the simulation grid. In addition, we know that the long-time concentration profile of c_A and c_B must be linear (satisfying the condition $\frac{\partial c^{ss}}{\partial t} = D^x \frac{\partial^2 c^{ss}}{\partial x^2} = 0$)

$$c_A^{ss}(x) = \frac{c_A^{bulk} - c_A^0}{L_x} x + c_A^0 \quad (42a)$$

$$c_B^{ss}(x) = \frac{c_B^{bulk} - c_B^0}{L_x} x + c_B^0 \quad (42b)$$

Finally, substituting eq 42a into eq 40 yields a steady-state concentration of

$$I_{ss} = \frac{n\mathcal{F}AD_A^x(c_A^{bulk} - c_A^0)}{L_x} \approx \frac{n\mathcal{F}AD_A^x c_A^{bulk}}{L_x} \frac{e^{-\beta\Delta G}}{1 + e^{-\beta\Delta G}} \quad (43)$$

since $c_A^0 \approx c_A^{bulk} \frac{1}{1 + e^{-\beta\Delta G}}$ when $c_B^{bulk} = 0$.

A similar analysis can be done using the difference in forward and backward rates, eq 17b, for the current

$$I_{ss} = n\mathcal{F}A(k_f c_A^{ss} - k_b c_B^{ss})|_{x=0}$$

$$I_{ss} = \frac{n\mathcal{F}A\Gamma}{\hbar} e^{-\alpha\beta\Delta G}(c_A^0 - c_B^0 e^{\beta\Delta G}) \quad (44)$$

Insertion of eq 41 for c_A^0 into eq 44 (and assuming $c_B^0 \approx c_A^{bulk} \frac{e^{-\beta\Delta G}}{1 + e^{-\beta\Delta G}}$) yields

$$I_{ss} = \frac{n\mathcal{F}A\Gamma}{\hbar} e^{-\alpha\beta\Delta G}(c_B^0(e^{\beta\Delta G} + \kappa) - c_B^0 e^{\beta\Delta G})$$

$$I_{ss} = \frac{n\mathcal{F}A\Gamma}{\hbar} e^{-\alpha\beta\Delta G}\kappa c_B^0 \approx \frac{n\mathcal{F}A\Gamma}{\hbar} e^{-\alpha\beta\Delta G}\kappa c_A^{bulk} \frac{e^{-\beta\Delta G}}{1 + e^{-\beta\Delta G}} \quad (45)$$

Comparison of eqs 43 and 45 shows that $\kappa = \frac{\hbar D_x e^{\alpha\beta\Delta G}}{\Gamma L_x}$ for the case where $c_B^{bulk} = 0$, such that $c_B^0 = c_A^{bulk} - c_A^0$.

Figure 10 and eq 43 demonstrate that in the long-time limit, where mass diffusion is rate-limiting, the steady-state current is actually independent of the coupling strength[f]. That being said, Figure 10 and eq 43 also show a fundamental artifact of all electrochemical simulations using eqs 17a, 17b, 26a, and 26b; steady-state current should not depend on the choice of the grid. The problem of grid length has been previously recognized for unequally spaced grids,[43−45] and the general boundary flux problem is known to have a simulation box size dependence.[46−48] Looking forward, our belief is that an accurate treatment of electrostatic interactions in simulations should mitigate the aberrant behavior shown in Figure 10, such that the steady-state solution for $c_A(x)$ and $c_B(x)$ will not necessarily be linear between 0 and L (eqs 42a and 42b), and our modeling should be more accurate at long times. Including these electrostatic interactions within the surface hopping framework will be the focus of the ongoing work. Note that one straightforward way of incorporating the electrical double layer into this formalism is by adding $\pm e\psi(x, \Delta G)$ to ΔG, where $\psi(x, \Delta G)$ is the electrostatic potential at a distance x from the electrode with applied potential ΔG and is often modeled as dropping linearly over the inner and/or outer Helmholtz layers.[1,49]

4.2. Coarse-Graining Ab Initio Rate Constants. The final issue we would like to address in this paper is the question of how we might parameterize the rate constants k_f and k_b in eqs 6a, 6b, 21a, 21b, 28a, and 28b. Throughout this paper, we have assumed that Γ is equal to a certain value at $x = 0$ and zero for all other x. Of course, in reality, Γ should vary smoothly in the x-direction. Thus, how should we construct $\Gamma(x)$ in practice?

In Figure 11, we carried out simulations using eqs 12a and 12b but on a much denser grid ($N_x = 500$) where Γ is a smooth function of x

$$\Gamma(x) = \Gamma_0' e^{-x/\lambda} \quad (46)$$

In Figure 11, we also plot electrochemical simulations with $N_x = 50$ using $\Gamma(x) = \Gamma_0\delta(x)$, where $\Gamma_0 \equiv \Gamma_0'\lambda$. From the results shown in Figure 11, simulations with dense or sparse grids yield equivalent answers, as long as λ is small enough such that there is no appreciable ability to hop beyond the first grid point in the more sparse simulation. Thus, altogether, the data in Figure 11 suggests that if one can compute an ab initio reaction rate $k_f(x)$ for a species near a metal surface, one needs only to calculate

$$k_f = \int_0^\infty k_f(x)dx \quad (47)$$

to parameterize a 1D model for the electrochemical dynamics ($x = 0$ represents the metal surface). We remind the reader that the final k_f value will, in fact, have units of cm/s compared to the ab initio reaction rate $k_f(x)$, which has units of s^{-1}. This simple relationship in eq 47 opens up many avenues for future explorations. Note that the distance-dependence of the coupling and the electrostatic potential term from an electrical double layer model may exert counteracting effects, leading to interesting dynamics in the region near the electrode surface.[49]

5. CONCLUSIONS

In this paper, we have (1) shown the equivalence of the surface hopping approach with traditional electrochemical methods and (2) quantified instances under which a 2D surface hopping model can or cannot be marginalized to a simpler 1D MH model. Regarding the latter question, we find that the key

DOI: 10.1021/acs.jpcc.9b02068
J. Phys. Chem. C 2019, 123, 13304−13317

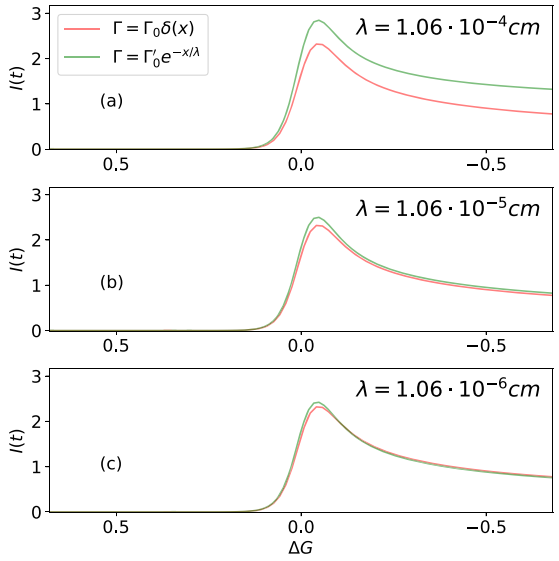


Figure 11. Linear sweep voltammograms for simulations with two different types of x dependence for Γ, $\Gamma(x) = \Gamma_0' e^{-x/\lambda}$ (eq 46), $\Gamma(x) = \Gamma_0 \delta(x)$ (eqs 12a and 12b), and we fix $\Gamma_0 = \frac{\Gamma_0'}{\lambda}$. $\Delta G_i = 0.816$ V, $\Delta G_f = -0.816$ V, $D = 5.5 \times 10^{-4}$ cm^2/s, $\frac{\Gamma_0}{\hbar} = 1.40 \times 10^8$ cm/s, and $\nu = 112$ V/s for each subplot. $N_x = 500$ for the $\Gamma(x) = \Gamma_0' e^{-x/\lambda}$ model and $N_x = 50$ for the $\Gamma(x) = \Gamma_0 \delta(x)$ model. (a) $\lambda = 1.06 \times 10^{-4}$ cm, (b) $\lambda = 1.06 \times 10^{-5}$ cm (c) $\lambda = 1.06 \times 10^{-6}$ cm. The results in (a) show the case where appreciable hopping occurs past the first grid point in the more sparse simulation, illustrating the breakdown of the δ-function approximation. Overall, this data confirms how one should construct Γ_0 for a sparse grid so as to match ab initio rate constants which drop off with length $\frac{1}{\lambda}$ from the surface.

consideration is one of the separability: If the solvent reorganization coordinate (ζ) and the diffusion coordinate (x) are nearly separable, a 1D MH model is good enough, and when compared with a multidimensional approach, the 1D MH is far more reliable than the Butler–Volmer or Nernstian dynamics. Nevertheless, if there is no separability between ζ and x, a 2D treatment is necessary and can be easily accomplished with a multidimensional SH approach.

Looking forward, if one seeks to model I–V curves under external potentials, the new approaches presented here should be of a great value. After all, current voltammetry simulation packages, such as DigiElch,[50] usually assume 1D systems with predetermined rate constants, chosen as linearized Marcus rates (as one would usually associate with the Butler–Volmer dynamics) or full Marcus rates (which, if calculated properly, should come from averaging over solvent fluctuations, as in eqs 28a and 28b). By contrast, our guiding principle is that the time has come to utilize modern nonadiabatic dynamics algorithms to study electrochemical ET for arbitrary PESs. Using the simple analysis in the Discussion section, our hope is that in the near future, we will be able to simulate unknown mechanistic pathways for unexplained chemical systems, with realistic parameters taken from ab initio DFT studies.

■ ASSOCIATED CONTENT

Supporting Information

The Supporting Information is available free of charge on the ACS Publications website at DOI: 10.1021/acs.jpcc.9b02068.

Information pertaining to numerical simulation details for the diagonalization of the Fokker–Planck operator, further analysis of nonseparable 2D Hamiltonians, and how to determine surface concentrations in traditional 1D Nerstian and Butler–Volmer simulations (PDF)

■ AUTHOR INFORMATION

Corresponding Author

*E-mail: alecja@sas.upenn.edu.

ORCID

Alec J. Coffman: 0000-0001-6764-4036

Sharon Hammes-Schiffer: 0000-0002-3782-6995

Notes

The authors declare no competing financial interest.

■ ACKNOWLEDGMENTS

We thank Abe Nitzan, Alexander Soudackov, and Adam Willard for very helpful conversations. This material is based upon work supported by the Air Force Office of Scientific Research (AFOSR) under award number FA9550-18-1-0420.

■ ADDITIONAL NOTES

[a]Interestingly, although this manuscript will not address the dynamics in the adiabatic representation, for E defined in eqs 9a, 9b, 9c, 9d, and 9e, if one commits to the adiabatic representation, the electronic friction tensor here arises exclusively from non-Condon effects (i.e., the electronic friction tensor is proportional to $\frac{\partial \Gamma}{\partial \vec{r}}$). For details, see ref 33.

[b]In other words, for SH, the relevant boundary conditions are $\frac{\partial c_A}{\partial x}|_{x=0^-} = \frac{\partial c_B}{\partial x}|_{x=0^-}$.

[c]Note that the mathematics in this section can be safely skipped by the reader who is not concerned about the stability of diagonalizing a non-Hermitian matrix. For the practical reader, who wants to repeat our calculations, however, these details will be essential.

[d]In this paper, if we do not use enough grid points, we must sometimes force the lowest eigenvalue to be equal to zero for the numerical stability.

[e]The transfer coefficient α represents the slope of the log current with respect to the external potential, ΔG, at the zero external potential, i.e., $\alpha = -kT \frac{\partial \log(I)}{\partial \Delta G}|_{\Delta G = \Delta G^\circ}$.[26]

[f]Note that this long-time simulation is not equivalent to a Tafel measurement. For the present paper, we allow the concentrations of A and B to change at the electrode surface subject to diffusion, as to study the effect of the mass transfer on the voltammetry curves. By contrast, for a Tafel plot, one works under the assumption that the concentrations of A and B are largely fixed at the electrode surface and are not affected by diffusion.

■ REFERENCES

(1) Bard, A. J.; Faulkner, L. R. *Electrochemical Methods: Fundamentals and Applications*; Wiley: New York, 2001.

(2) Yan, D.; Bazant, M. Z.; Biesheuvel, P. M.; Pugh, M. C.; Dawson, F. P. Theory of linear sweep voltammetry with diffuse charge: Unsupported electrolytes, thin films, and leaky membranes. *Phys. Rev. E* **2017**, *95*, No. 033303.

(3) Smalley, J. F.; Chidsey, C. E. D.; Creager, S. E.; Ferraris, J. P.; Finklea, H. O.; Chalfant, K.; Zawodzinsk, T.; Newton, M. D.; Feldberg, S. W.; Linford, M. R. Heterogeneous Electron-Transfer

DOI: 10.1021/acs.jpcc.9b02068
J. Phys. Chem. C 2019, 123, 13304–13317

Kinetics for Ruthenium and Ferrocene Redox Moieties through Alkanethiol Monolayers on Gold. *J. Am. Chem. Soc.* **2003**, *125*, 2004−2013.
(4) Feldberg, S. W. Implications of marcus-hush theory for steady-state heterogeneous electron transfer at an inlaid disk electrode. *Anal. Chem.* **2010**, *82*, 5176−5183.
(5) Henstridge, M. C.; Laborda, E.; Rees, N. V.; Compton, R. G. Marcus-Hush-Chidsey theory of electron transfer applied to voltammetry: A review. *Electrochim. Acta* **2012**, *84*, 12−20.
(6) Laborda, E.; Henstridge, M. C.; Batchelor-McAuley, C.; Compton, R. G. Asymmetric Marcus-Hush theory for voltammetry. *Chem. Soc. Rev.* **2013**, *42*, 4894.
(7) Matyushov, D. V.; Newton, M. D. Q-model of electrode reactions: altering force constants of intramolecular vibrations. *Phys. Chem. Chem. Phys.* **2018**, *20*, 24176−24185.
(8) Oldham, K. B.; Myland, J. C. On the evaluation and analysis of the Marcus-Hush-Chidsey integral. *J. Electroanal. Chem.* **2011**, *655*, 65−72.
(9) Migliore, A.; Nitzan, A. On the evaluation of the Marcus-Hush-Chidsey integral. *J. Electroanal. Chem.* **2012**, *671*, 99−101.
(10) Henstridge, M. C.; Laborda, E.; Wang, Y.; Suwatchara, D.; Rees, N.; Molina, Á.; Martínez-Ortiz, F.; Compton, R. G. Giving physical insight into the Butler-Volmer model of electrode kinetics: Application of asymmetric Marcus-Hush theory to the study of the electroreductions of 2-methyl-2-nitropropane, cyclooctatetraene and europium(III) on mercury microelectrodes. *J. Electroanal. Chem.* **2012**, *672*, 45−52.
(11) Henstridge, M. C.; Laborda, E.; Dickinson, E. J. F.; Compton, R. G. Redox systems obeying Marcus-Hush-Chidsey electrode kinetics do not obey the Randles-Ševčík equation for linear sweep voltammetry. *J. Electroanal. Chem.* **2012**, *664*, 73−79.
(12) Tanner, E. E.; Xiong, L.; Barnes, E. O.; Compton, R. G. One electron oxygen reduction in room temperature ionic liquids: A comparative study of Butler-Volmer and Symmetric Marcus-Hush theories using microdisc electrodes. *J. Electroanal. Chem.* **2014**, *727*, 59−68.
(13) Okajima, Y.; Shibuta, Y.; Suzuki, T. A phase-field model for electrode reactions with Butler-Volmer kinetics. *Comput. Mater. Sci.* **2010**, *50*, 118−124.
(14) Skúlason, E.; Tripkovic, V.; Björketun, M. E.; Gudmundsdóttir, S.; Karlberg, G.; Rossmeisl, J.; Bligaard, T.; Jónsson, H.; Nørskov, J. K. Modeling the electrochemical hydrogen oxidation and evolution reactions on the basis of density functional theory calculations. *J. Phys. Chem. C* **2010**, *114*, 18182−18197.
(15) Roldan, A. Frontiers in first principles modelling of electrochemical simulations. *Curr. Opin. Electrochem.* **2018**, *10*, 1−6.
(16) Zusman, L. D. Outer-sphere electron transfer in polar solvents. *Chem. Phys.* **1980**, *49*, 295−304.
(17) Rips, I.; Jortner, J. Dynamic solvent effects on outer-sphere electron transfer. *J. Chem. Phys.* **1987**, *87*, 2090−2104.
(18) Straub, J. E.; Berne, B. J. A statistical theory for the effect of nonadiabatic transitions on activated processes. *J. Chem. Phys.* **1987**, *87*, 6111−6116.
(19) Matyushov, D. V.; Schmid, R. A molecular treatment of solvent effects on intervalence electron transfer. *J. Phys. Chem.* **1994**, *98*, 5152−5159.
(20) Dorfman, R. C.; Fayer, M. D. The influence of diffusion on photoinduced electron transfer and geminate recombination. *J. Chem. Phys.* **1992**, *96*, 7410−7422.
(21) Gladkikh, V. S.; Burshtein, A. I.; Tavernier, H. L.; Fayer, M. D. Influence of diffusion on the kinetics of donor-acceptor electron transfer monitored by the quenching of donor fluorescence. *J. Phys. Chem. A* **2002**, *106*, 6982−6990.
(22) Gladkikh, V.; Burshtein, A. I.; Feskov, S. V.; Ivanov, A. I.; Vauthey, E. Hot recombination of photogenerated ion pairs. *J. Chem. Phys.* **2005**, *123*, No. 244510.
(23) Bai, P.; Bazant, M. Z. Charge transfer kinetics at the solid-solid interface in porous electrodes. *Nat. Commun.* **2014**, *5*, No. 3585.
(24) Reed, S. K.; Madden, P. A.; Papadopoulos, A. Electrochemical charge transfer at a metallic electrode: A simulation study. *J. Chem. Phys.* **2008**, *128*, No. 124701.
(25) Tully, J. C. Molecular dynamics with electronic transitions. *J. Chem. Phys.* **1990**, *93*, 1061−1071.
(26) Schmickler, W.; Santos, E. *Interfacial Electrochemistry*; Springer-Verlag: Berlin, 2010.
(27) Randles, J. E. A cathode ray polarograph. Part II. - The current-voltage curves. *Trans. Faraday Soc.* **1948**, *44*, 327−338.
(28) Ševčík, A. Oscillographic polarography with periodical triangular voltage. *Collect. Czech. Chem. Commun.* **1948**, *13*, 349−377.
(29) Nicholson, R. S.; Shain, I. Theory of Stationary Electrode Polarography: Single Scan and Cyclic Methods Applied to Reversible, Irreversible, and Kinetic Systems. *Anal. Chem.* **1964**, *36*, 706−723.
(30) Matsuda, H.; Ayabe, Y. Zur Theorie der Randles Sevčikschen Kathodenstrahl Polarographie. *Z. Electrochem.* **1955**, *59*, 494−503.
(31) Nicholson, R. S. Theory and Application of Cyclic Voltammetry for Measurement of Electrode Reaction Kinetics. *Anal. Chem.* **1965**, *37*, 1351−1355.
(32) Myland, J. C.; Oldham, K. B. An analytical expression for the current-voltage relationship during reversible cyclic voltammetry. *J. Electroanal. Chem.* **1983**, *153*, 43−54.
(33) Dou, W.; Subotnik, J. E. Electronic friction near metal surfaces: A case where molecule-metal couplings depend on nuclear coordinates. *J. Chem. Phys.* **2017**, *146*, No. 092304.
(34) Dou, W.; Nitzan, A.; Subotnik, J. E. Surface hopping with a manifold of electronic states. II. Application to the many-body Anderson-Holstein model. *J. Chem. Phys.* **2015**, *142*, No. 084110.
(35) Marcus, R. A. On the Theory of Electron-Transfer Reactions. VI. Unified Treatment for Homogeneous and Electrode Reactions. *J. Chem. Phys.* **1965**, *43*, 679−701.
(36) Dou, W.; Subotnik, J. E. A broadened classical master equation approach for nonadiabatic dynamics at metal surfaces: Beyond the weak molecule-metal coupling limit. *J. Chem. Phys.* **2016**, *144*, No. 024116.
(37) Compton, R. G.; Laborda, E.; Ward, K. R. *Understanding Voltammetry*; Imperial College Press, 2014.
(38) Press, W. H.; Teukolsky, S. A.; Vetterling, W. T.; Flannery, B. P. *Numerical Recipes in C: The Art of Scientific Computing*; Cambridge University Press, 1992.
(39) Hull, T. E.; Enright, W. H.; Fellen, B. M.; Sedgwick, A. E. Comparing Numerical Methods for Ordinary Differential Equations. *SIAM J. Numer. Anal.* **1972**, *9*, 603−637.
(40) Brown, P. N.; Byrne, G. D.; Hindmarsh, A. C. VODE: A Variable-Coefficient ODE Solver. *SIAM J. Sci. Stat. Comput.* **1989**, *10*, 1038−1051.
(41) Jung, Y. J.; Cao, J. Spectral analysis of electron transfer kinetics II. *J. Chem. Phys.* **2002**, *117*, 3822−3836.
(42) Risken, H. *The Fokker-Planck Equations, Method of Solution and Applications*, 2nd ed.; Springer-Verlag, 1989; p 103.
(43) Rudolph, M. Digital simulations on unequally spaced grids. Part 1. Critical remarks on using the point method by discretisation on a transformed grid. *J. Electroanal. Chem.* **2002**, *529*, 97−108.
(44) Rudolph, M. Digital simulations on unequally spaced grids. Part 2. Using the box method by discretisation on a transformed equally spaced grid. *J. Electroanal. Chem.* **2003**, *543*, 23−39.
(45) Rudolph, M. Digital simulations on unequally spaced grids. Part 3. Attaining exponential convergence for the discretisation error of the flux as a new strategy in digital simulations of electrochemical experiments. *J. Electroanal. Chem.* **2004**, *571*, 289−307.
(46) Rudolph, M. Attaining exponential convergence for the flux error with second- and fourth-order accurate finite-difference equations. I. Presentation of the basic concept and application to a pure diffusion system. *J. Comput. Chem.* **2005**, *26*, 619−632.
(47) Rudolph, M. Attaining exponential convergence for the flux error with second- and fourth-order accurate finite-difference equations. II. Application to systems comprising first-order chemical reactions. *J. Comput. Chem.* **2005**, *26*, 633−641.

DOI: 10.1021/acs.jpcc.9b02068
J. Phys. Chem. C 2019, 123, 13304−13317

(48) Rudolph, M. Attaining exponential convergence for the flux error with second- and fourth-order accurate finite-difference equations. Part 3. Application to electrochemical systems comprising second-order chemical reactions. *J. Comput. Chem.* **2005**, *26*, 1193−1204.
(49) Goldsmith, Z. K.; Lam, Y. C.; Soudackov, A. V.; Hammes-Schiffer, S. Proton discharge on a gold electrode from triethylammonium in acetonitrile: Theoretical modeling of potential-dependent kinetic isotope effects. *J. Am. Chem. Soc.* **2019**, *141*, 1084−1090.
(50) Rudolph, M.; Reddy, D. P.; Feldberg, S. W. A Simulator for Cyclic Voltammetric Responses. *Anal. Chem.* **1994**, *66*, 589A−600A.

DOI: 10.1021/acs.jpcc.9b02068
J. Phys. Chem. C 2019, 123, 13304−13317